Application of Continnuumnization for Predicting Dynamic Properties of Brick Mortar Systems

Sumet SUPPRASERT*, Lalith WIJERATHNE**, Jian CHEN***, Muneo HORI**** and Tsuyoshi ICHIMURA†

*PhD. Candidate, Department of Civil Engineering, University of Tokyo (Bunkyo, Tokyo 113-0032)
**Associate Professor, Earthquake Research Institute, University of Tokyo (Bunkyo, Tokyo 113-0032)
***Dr. of Eng. Research Associate, RIKEN AICS (Minatoshima-Minami, Kobe 650-0047)
****Professor, Earthquake Research Institute, University of Tokyo (Bunkyo, Tokyo 113-0032)
†Associate Professor, Earthquake Research Institute, University of Tokyo (Bunkyo, Tokyo 113-0032)

We developed equivalent continuum forms for brick structures based on continuumnization by Hori et al. Approximating the discrete vector fields with Taylor series expansion, we obtained two continnumnized models for predicting wave properties; the first model is based on second order approximation, while the other uses infinite series. With numerical simulations, we demonstrate that continuumnization can accurately predict the properties of p-, s- and rotational waves making it good tool for verification of rigid body spring model (RBSM) based codes. It is demonstrated that the second order model can predict wave properties for a reasonably wide range of wave numbers, while the model based on infinite series can make accurate predictions even for high frequency applications. Further, a preliminary investigation is conducted on the possible contribution from predicted high speed spins to damping of brick mortar or granule systems.

Key Words: *brick structures, continuumnization, dynamic charateristics, rotational-waves, damping*

1. Introduction

Brick structures are often modeled as rigid-body-spring systems, assuming that each brick-unit is a rigid block and mortar is infinitesimal springs[2),3),4),5),6),7)]. Such discrete models are convenient for simulating brick structures, including damage and nonlinear mortar behavior. However, when it come to the design of structures, rigid-body-spring systems are quite inconvenient. For design purposes, what the desired are some analytical relations for predicting the properties of discrete system and simplified numerical models like beams and shells in structural mechanics. Though FEM models for brick structures have been developed based on homogenization techniques[8),9)], their accuracy is low. Further, analytical tools for accurately predicting dynamic properties of discrete system is invaluable in verification of numerical codes based on rigid-body-spring or similar techniques.

The method of *continuumnization,* proposed by Hori et al.[1)], is an ideal tool for deriving equivalent continuum form of governing equations for regularly packed discrete systems like gralue systems, masonry structures, etc. The resulting continuumnized governing equations can be used either to predict dynamic properties of the discrete system, or use numerical techniques in continuum mechanics to analyze discrete systems. Hori et al. has applied continuumnization to predict wave characteristics of 2D regularly packed rigid sphere network connected with springs.

In this work we apply the continuumnization to predict wave characteristics of brick-mortar systems targeting applications in brick structure designs and verification of numerical codes for simulating brick structures. We use Taylor series expansion to obtain the continuum governing equations for the discrete system. In their original work, Hori et al.[1)] have made use of the difference operator in deriving the continuum forms. In some sense, the Taylor series based approach is quite similar to the difference operator based approach. However, the Taylor series approach allows one to obtain characteristic equations of arbitrary higher order, which allows to accurately predict the wave properties for a wider range of wave numbers.

Approximating the discrete vector fields with Taylor series expansion, we obtained two continuumnized models for predicting wave properties. The first model is uses Taylor series truncated at second order terms, while second model use the whole Taylor series to approximate discrete vector filed. With a set of numerical simulations, it is demonstrated that continuumnization can accurately predict the properties of p-, s- and rotational waves making it good tool for verification of RBSM codes. It is demonstrated that the second order model is valid for a reasonable range of wave numbers, while the model based on the infinite series significantly expand the range of applicability.

It was hypothesized by Hori et al.[1)] that the high speed spins predicted by continnumined equation of motion can be a source of damping in granule or brick systems. We conducted a preliminary study to investigate the possible contribution from predicted high speed spins to damping of brick mortar or granule systems. It is demonstrated that rapid decay of high predicted high speed spin and the interplay between translation and rotation mode can produce significant energy loss and damping of translational responses. However, further investigations are necessary to conclude the contribution of predicted high speed spin on system damping.

The rest of the paper is organized as follows. The second section presents the derivations of continnumnied equation of motions and charateristic equations for predicting wave properties for regularly packed brick motar systems. The third section investigates the range of applicability of each continnumnized model derived in the section 2. The fourth section presents the priliminary study on the contribution of the predicted high speed spins on the damping of brick motar system. The last section provides some concluding remarks.

2. Continuumnization of a regularly packed brick system

Often in engineering applications, it is important to know how the dynamic characteristics like wave speeds vary with brick size, brick arrangement and material properties. The discrete equations of motion, Eq.(4), is inconvenient for such application. Surely, one can do a large number of simulations varying the required parameters and obtain some relations among the required parameters. Instead of such brute force approach, we can use the continuumnization proposed by Hori et al.[1)] to study system characteristics analytically. Continuumnization allows one to pose a set of partial differential equations based on the discrete equations of motion. This continuum form has several advantages: can be used to analytically study the above mentioned wave characteristics of the system; make it possible to apply FEM or other numerical methods in continuum mechanics for simulating brick structure; make it possible to develop dimension reduced models, like beam and shells in structural mechanics, for brick structure analysis; etc.

2.1 Regularly packed bricks as a discrete system

As the starting point to derive the equivalent continuum form of equations of motion, the discrete equations of motion for a regularly packed brick mortar system is obtained. We idealize a single layer brick wall as a network of rigid rectangular blocks connected with infinitesimally short linear elastic springs, as shown in Fig.1(a). The springs represent elasticity of both the bricks and mortar layers, while the domain of each rigid blocks include a portion of cement layers so that the domain occupied by the brick mortar system is perfectly tessellated.

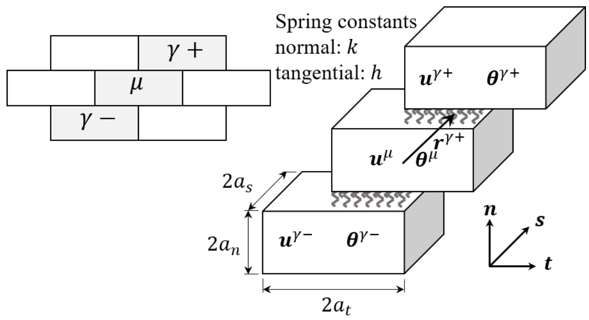

(a) Neighboring blocks of regularly packed bricks

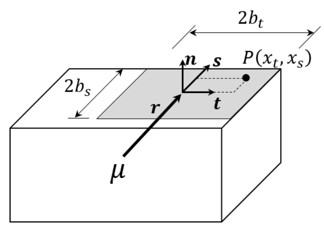

(b) Contact area of two neighboring blocks

Fig. 1: Idealized block-spring model.

Lets consider an arbitrary block μ, located at $\boldsymbol{x}^{\mu}$, of a regularly packed brick mortar system (see Fig. 1(a). Depending on the regular packing, it can have several even number of neighbors. In identifying the neighbors, we group them as pairs. The two neighbors located either sides in the γ^{th} direction, $\boldsymbol{r}^{\gamma}$, are denoted as $\gamma\pm$, and their centroids are $\boldsymbol{x}^{\mu}\pm 2\boldsymbol{r}^{\gamma\pm}$. Let $\boldsymbol{n}^{\gamma}$, $\boldsymbol{t}^{\gamma}$ and $\boldsymbol{s}^{\gamma}$ be an orthonormal coordinate system on contact area with the neighboring block in $\boldsymbol{r}^{\gamma}$ direction. As shown in Fig. 1(b) the origin is located at the centroid of the contact area. For the sake of simplicity, we omit the superscript and write these directions as $\boldsymbol{n}$, $\boldsymbol{t}$ and $\boldsymbol{s}$. Let the dimension of this rectangular contact area be $2b_t$ and $2b_s$. Note that $\boldsymbol{r}^{\gamma\pm}$ denote the relative position of the centroid of the contact areas with the neighbors $\gamma\pm$. An arbitrary point on the contact area can be represented as (x_t,x_s), with respect to this local coordinate system.

Assume that the bricks are rigid and undergo infinitesimally small deformation. Let the translation and rotation of μ^{th} block be $\boldsymbol{u}^{\mu}$ and $\boldsymbol{\theta}^{\mu}$, while those of neighbors are $\boldsymbol{u}^{\gamma\pm}$ and $\boldsymbol{\theta}^{\gamma\pm}$. The resulting relative displacement at the a point (x_t,x_s) on the contact area with the neighbor $\gamma+$ can be expressed as

$$\begin{aligned}\boldsymbol{L}^{\gamma+}=&\left(\boldsymbol{u}^{\gamma+}-\boldsymbol{u}^{\mu}\right)-\left(\boldsymbol{\theta}^{\gamma+}+\boldsymbol{\theta}^{\mu}\right)\times\boldsymbol{r}^{\gamma+}\\&+\left(\boldsymbol{\theta}^{\gamma+}-\boldsymbol{\theta}^{\mu}\right)\times(x_t\boldsymbol{t}+x_s\boldsymbol{s}).\end{aligned}\tag{1}$$

If k and h are the normal and tangential spring constants, respectively, the elastic energy stored in the spring due to the relative deformation $\boldsymbol{L}^{\gamma+}$ is

$$\begin{aligned}V^{\mu\gamma+}=&\frac{1}{2}\iint k\left(\boldsymbol{n}\cdot\boldsymbol{L}^{\gamma+}\right)^2\\&+h\left\{\left(\boldsymbol{t}\cdot\boldsymbol{L}^{\gamma+}\right)^2+\left(\boldsymbol{s}\cdot\boldsymbol{L}^{\gamma+}\right)^2\right\}\mathrm{d}x_s\mathrm{d}x_t.\end{aligned}\tag{2}$$

The Lagrangian for the whole discrete system is

$$\mathcal{L}=\sum_{\mu}\left(\frac{1}{2}m\dot{\boldsymbol{u}}^{\mu}\cdot\dot{\boldsymbol{u}}^{\mu}+\frac{1}{2}\dot{\boldsymbol{\theta}}^{\mu}\cdot\boldsymbol{I}\cdot\dot{\boldsymbol{\theta}}^{\mu}-V^{\mu}\right),\tag{3}$$

where $V^{\mu}=\sum_{\gamma}(V^{\mu\gamma+}+V^{\mu\gamma-})$. m and $\boldsymbol{I}$ are the mass and inertia tensor of each block.

Applying the Hamilton's principal of stationary action, $\delta\int\mathcal{L}\mathrm{d}t=0$, we can obtain the following discrete equations of motion

$$\begin{aligned}m\ddot{\boldsymbol{u}}^{\mu}=&\sum_{\gamma}\Big\{\boldsymbol{K}^{\mu\gamma}\cdot\left(\boldsymbol{u}^{\gamma+}-2\boldsymbol{u}^{\mu}+\boldsymbol{u}^{\gamma-}\right)\\&-\hat{\boldsymbol{K}}^{\mu\gamma}\cdot\left(\boldsymbol{\theta}^{\gamma+}-\boldsymbol{\theta}^{\gamma-}\right)\Big\}\\ \boldsymbol{I}\cdot\ddot{\boldsymbol{\theta}}^{\mu}=&\sum_{\gamma}\Big\{\left(\hat{\boldsymbol{K}}^{\mu\gamma}\right)^{\mathrm{T}}\cdot\left(\boldsymbol{u}^{\gamma+}-\boldsymbol{u}^{\gamma-}\right)\\&-\overline{\boldsymbol{K}}^{\mu\gamma}\cdot\left(\boldsymbol{\theta}^{\gamma+}+2\boldsymbol{\theta}^{\mu}+\boldsymbol{\theta}^{\gamma-}\right)\\&+\overline{\overline{\boldsymbol{K}}}^{\mu\gamma}\cdot\left(\boldsymbol{\theta}^{\gamma+}-2\boldsymbol{\theta}^{\mu}+\boldsymbol{\theta}^{\gamma-}\right)\Big\},\end{aligned}\tag{4}$$

where

$$\begin{aligned}\boldsymbol{K}^{\mu\gamma}=&4b_tb_s\left(k\boldsymbol{n}\otimes\boldsymbol{n}+h\boldsymbol{t}\otimes\boldsymbol{t}+h\boldsymbol{s}\otimes\boldsymbol{s}\right)\\ \hat{\boldsymbol{K}}^{\mu\gamma}=&4b_tb_s\left\{k\boldsymbol{n}\otimes(\boldsymbol{r}\times\boldsymbol{n})+h\boldsymbol{t}\otimes(\boldsymbol{r}\times\boldsymbol{t})\right.\\&\left.+h\boldsymbol{s}\otimes(\boldsymbol{r}\times\boldsymbol{s})\right\}\\ \overline{\boldsymbol{K}}^{\mu\gamma}=&4b_tb_s\left\{k(\boldsymbol{r}\times\boldsymbol{n})\otimes(\boldsymbol{r}\times\boldsymbol{n})\right.\\&\left.+h(\boldsymbol{r}\times\boldsymbol{t})\otimes(\boldsymbol{r}\times\boldsymbol{t})+h(\boldsymbol{r}\times\boldsymbol{s})\otimes(\boldsymbol{r}\times\boldsymbol{s})\right\}\\ \overline{\overline{\boldsymbol{K}}}^{\mu\gamma}=&\frac{4}{3}\left\{h\left(b_tb_s^3+b_t^3b_s\right)\boldsymbol{n}\otimes\boldsymbol{n}+kb_tb_s^3\boldsymbol{t}\otimes\boldsymbol{t}\right.\\=&\left.+kb_t^3b_s\boldsymbol{s}\otimes\boldsymbol{s}\right\}.\end{aligned}$$

The matrices $\boldsymbol{K}^{\mu\gamma}$,$\hat{\boldsymbol{K}}^{\mu\gamma}$, $\overline{\boldsymbol{K}}^{\mu\gamma}$ and $\overline{\overline{\boldsymbol{K}}}^{\mu\gamma}$ define different modes of interaction between neighboring blocks. It is $\hat{\boldsymbol{K}}^{\mu\gamma}$ which couples translations and rotations. The above obtained equations of motion for the discrete system can be used to simulate a brick structure as a mass spring system, in which the $\boldsymbol{K}^{\mu\gamma}$, $\hat{\boldsymbol{K}}^{\mu\gamma}$, $\overline{\boldsymbol{K}}^{\mu\gamma}$and $\overline{\overline{\boldsymbol{K}}}^{\mu\gamma}$defines spring constants for the interactions among different degrees of freedoms.

2.2 Continuumnization

In their original work, Hori et al. obtained the equivalent continuum form by assuming the presence of smooth vector fields $\boldsymbol{u}$ and $\boldsymbol{\theta}$ and approximating the differences of discrete terms $\boldsymbol{u}^{\gamma\pm}-\boldsymbol{u}^{\mu}$ and $\boldsymbol{\theta}^{\gamma\pm}-\boldsymbol{\theta}^{\mu}$ based on the difference operator. In this paper, we use Taylor series expansion to obtain the continuum form. In some sense the use of Taylor series expansion is quite similar to using difference operators. However, the Taylor series approach allows one to obtain characteristic equations of arbitrary higher order, which allows to accurately predict the wave properties for a wider range of wave numbers.

Lets assume that there exists two smooth vector fields $\boldsymbol{u}(\boldsymbol{x})$ and $\boldsymbol{\theta}(\boldsymbol{x})$ which satisfies $\boldsymbol{u}^{\mu}=\boldsymbol{u}(\boldsymbol{x}^{\mu})$ and $\boldsymbol{\theta}^{\mu}=\boldsymbol{\theta}(\boldsymbol{x}^{\mu})$. We can approximate $\boldsymbol{u}^{\gamma\pm}$ and $\boldsymbol{\theta}^{\gamma\pm}$ using Taylor series expansion. As an example, $\boldsymbol{u}^{\gamma\pm}$ can be approximated as

$$\begin{aligned}\boldsymbol{u}^{\gamma\pm}\approx&\boldsymbol{u}^{\mu}\pm2r_i\left[\frac{\partial\boldsymbol{u}}{\partial x_i}\right]_{\boldsymbol{x}^{\mu}}+2r_ir_j\left[\frac{\partial^2\boldsymbol{u}}{\partial x_i\partial x_j}\right]_{\boldsymbol{x}^{\mu}}\\&\pm\frac{2^3r_ir_jr_k}{3!}\left[\frac{\partial^3\boldsymbol{u}(\boldsymbol{x})}{\partial x_i\partial x_j\partial x_k}\right]_{\boldsymbol{x}^{\mu}}+\dots\end{aligned}\tag{5}$$

Based on the above expression, we can approximate $(\boldsymbol{u}^{\gamma+}\pm\boldsymbol{u}^{\gamma-})$ and $(\boldsymbol{u}^{\gamma+}-\boldsymbol{u}^{\gamma-})$ as

$$\begin{aligned}\boldsymbol{u}^{\gamma+}+\boldsymbol{u}^{\gamma-}\approx&2\boldsymbol{u}^{\mu}+\frac{2^3r_ir_j}{2!}\left[\frac{\partial^2\boldsymbol{u}(\boldsymbol{x})}{\partial x_i\partial x_j}\right]_{\boldsymbol{x}^{\mu}}\\&+\frac{2^5r_ir_jr_kr_l}{4!}\left[\frac{\partial^4\boldsymbol{u}(\boldsymbol{x})}{\partial x_i\partial x_j\partial x_k\partial x_l}\right]_{\boldsymbol{x}^{\mu}}+\dots\\ \boldsymbol{u}^{\gamma+}-\boldsymbol{u}^{\gamma-}\approx&\left[\frac{\partial\boldsymbol{u}(\boldsymbol{x})}{\partial x_i}\right]_{\boldsymbol{x}^{\mu}}2^2r_i\\&+\frac{2^4r_ir_jr_k}{3!}\left[\frac{\partial^3\boldsymbol{u}(\boldsymbol{x})}{\partial x_i\partial x_j\partial x_k}\right]_{\boldsymbol{x}^{\mu}}+\dots\end{aligned}\tag{6}$$

Similarly, it is straight forward to express $\left(\boldsymbol{\theta}^{\gamma+}\pm\boldsymbol{\theta}^{\gamma-}\right)$. Based on these expressions for $(\boldsymbol{u}^{\gamma+}\pm\boldsymbol{u}^{\gamma-})$ and $\left(\boldsymbol{\theta}^{\gamma+}\pm\boldsymbol{\theta}^{\gamma-}\right)$, we can express the set of equations in terms of continuous vector fields $\boldsymbol{u}(\boldsymbol{x})$ and $\boldsymbol{\theta}(\boldsymbol{x})$.

(1) A second order approximation

Lets make second order approximations all the $(\boldsymbol{u}^{\gamma+}\pm\boldsymbol{u}^{\gamma-})$ and $\left(\boldsymbol{\theta}^{\gamma+}\pm\boldsymbol{\theta}^{\gamma-}\right)$ using Eq.(6) (i.e. neglecting the terms with derivatives of third or higher order). Substituting these second order approximations to Eq.(4), we can obtain the following continuumnized equations of motion

$$\begin{aligned}\frac{m}{V_b}\ddot{\boldsymbol{u}}=&\nabla\cdot(\boldsymbol{c}:\nabla\boldsymbol{u})-\boldsymbol{q}:\nabla\boldsymbol{\theta}\\ \frac{1}{V_b}\boldsymbol{I}\cdot\ddot{\boldsymbol{\theta}}=&\boldsymbol{q}^{\mathrm{T}}:\nabla\boldsymbol{u}-\boldsymbol{d}\cdot\boldsymbol{\theta}+\nabla\cdot(\boldsymbol{v}:\nabla\boldsymbol{\theta}),\end{aligned}\tag{7}$$

where V_b is the volume of a block. $\boldsymbol{c}$, $\boldsymbol{q}$, $\boldsymbol{d}$, and $\boldsymbol{v}$ are 4^{th}, 3^{rd}, 2^{nd}, and 4^{th}-order tensors composed of material and geometric (i.e. block geometry and packing) properties. Explicit expressions for these tensors are

$$
\begin{aligned}
\boldsymbol{c}=&\frac{16b_tb_s}{V_b}(k\boldsymbol{r}\otimes\boldsymbol{n}\otimes\boldsymbol{r}\otimes\boldsymbol{n}+h\boldsymbol{r}\otimes\boldsymbol{t}\otimes\boldsymbol{r}\otimes\boldsymbol{t}\\
&+h\boldsymbol{r}\otimes\boldsymbol{s}\otimes\boldsymbol{r}\otimes\boldsymbol{s})\\
\boldsymbol{q}=&\frac{16b_tb_s}{V_b}\{k\boldsymbol{n}\otimes\boldsymbol{r}\otimes(\boldsymbol{r}\times\boldsymbol{n})+h\boldsymbol{t}\otimes\boldsymbol{r}\otimes(\boldsymbol{r}\times\boldsymbol{t})\\
&+h\boldsymbol{s}\otimes\boldsymbol{r}\otimes(\boldsymbol{r}\times\boldsymbol{s})\}\\
\boldsymbol{d}=&\frac{16b_tb_s}{V_b}\{k(\boldsymbol{r}\times\boldsymbol{n})\otimes(\boldsymbol{r}\times\boldsymbol{n})+h(\boldsymbol{r}\times\boldsymbol{t})\otimes(\boldsymbol{r}\times\boldsymbol{t})\\
&+h(\boldsymbol{r}\times\boldsymbol{s})\otimes(\boldsymbol{r}\times\boldsymbol{s})\}\\
\boldsymbol{v}=&\frac{16}{V_b}\left\{h\left(\frac{b_tb_s^3}{3}+\frac{b_t^3b_s}{3}\right)\boldsymbol{r}\otimes\boldsymbol{n}\otimes\boldsymbol{r}\otimes\boldsymbol{n}\right.\\
&\left.+\frac{kb_tb_s^3}{3}\boldsymbol{r}\otimes\boldsymbol{t}\otimes\boldsymbol{r}\otimes\boldsymbol{t}+\frac{kb_t^3b_s}{3}\boldsymbol{r}\otimes\boldsymbol{s}\otimes\boldsymbol{r}\otimes\boldsymbol{s}\right\}\\
&-\frac{16b_tb_s}{V_b}\{k\boldsymbol{r}\otimes(\boldsymbol{r}\times\boldsymbol{n})\otimes\boldsymbol{r}\otimes(\boldsymbol{r}\times\boldsymbol{n})\\
&+h\boldsymbol{r}\otimes(\boldsymbol{r}\times\boldsymbol{t})\otimes\boldsymbol{r}\otimes(\boldsymbol{r}\times\boldsymbol{t})\\
&+h\boldsymbol{r}\otimes(\boldsymbol{r}\times\boldsymbol{s})\otimes\boldsymbol{r}\otimes(\boldsymbol{r}\times\boldsymbol{s})\}.
\end{aligned}
$$

In the original work by Hori et al., the term $\left(\boldsymbol{\theta}^{\gamma+}+2\boldsymbol{\theta}^{\mu}+\boldsymbol{\theta}^{\gamma-}\right)$ is approximated as $4\boldsymbol{\theta}^{\mu}$. However, in the above formulation all the terms up to the second order derivatives are included in approximating $\left(\boldsymbol{\theta}^{\gamma+}+2\boldsymbol{\theta}^{\mu}+\boldsymbol{\theta}^{\gamma-}\right)$. This includes the additional term $\nabla\cdot(\boldsymbol{v}:\nabla\boldsymbol{\theta})$ in the above obtained continuum form Eq.7. We refer the set of equations of motion obtained by approximating $\left(\boldsymbol{\theta}^{\gamma+}+2\boldsymbol{\theta}^{\mu}+\boldsymbol{\theta}^{\gamma-}\right)\approx4\boldsymbol{\theta}^{\mu}$ as theoriginal continuumnization while the Eq.7 as second order continuumnization. As it is shown in the next section, Eq.7 is capable of capturing the wave properties, especially the rotational wave, for a wider range of wave lengths compared to the original form of continnumnization.

(2) Estimation of wave properties

A major advantage of Eq.(7) is that it makes it possible to analytically study the dynamic characteristics of the approximated discrete system. As an example, consider the two dimensional single layered brick wall shown in Fig.2. For this given packing, we can evaluate the four tensors, $\boldsymbol{c}$, $\boldsymbol{q}$, $\boldsymbol{d}$, and $\boldsymbol{v}$, and obtain the equivalent continuum form of equations of motion (i.e. Eq. 7). Taking the Fourier transform of the resulting equations, with the kernel of $e^{\imath(\boldsymbol{\xi}\cdot\boldsymbol{x}-\omega t)}$, where $\boldsymbol{\xi}=\xi\{\cos\theta_\xi,\sin\theta_\xi\}$, and solving the resulting characteristic equations, the relations between the wave frequencies and wave number can be obtained. Specifically, the relations between frequencies and wave numbers of pressure, shear and rotational waves due to in-plane deformation are obtained. Since the system is anisotropic, the wave velocities depends on the direction of the propagating wave. For example, the wave velocities of primary wave (p-wave) and secondary wave (s-wave) can be expressed

Table 1: Wave velocities and corresponding modes $\{u_1,u_2,\theta_3\}$ for $\theta_\xi=90°$.

wave	velocity	mode shape
p	$\sqrt{\frac{2ka_2}{\rho}}$	$\{0,1,0\}$
s	$\sqrt{\frac{2ka_2\eta(1+4\eta\gamma)}{\rho(1+4\eta\gamma+4\eta\gamma^2)}}$	$\left\{1,0,-\frac{(1+4\eta\gamma)\xi\mathrm{i}}{1+4\eta\gamma+4\eta\gamma^2}\right\}$
r	-	$\{0,0,1\}$

Table 2: Wave velocities and corresponding modes $\{u_1,u_2,\theta_3\}$ for $\theta_\xi=0°$.

wave	velocity	mode shape
p	$\sqrt{\frac{ka_2(\eta+4\gamma)}{2\rho\gamma^2}}$	$\{1,0,0\}$
s	$\sqrt{\frac{2ka_2\eta(1+4\eta\gamma)}{\rho(1+4\eta\gamma+4\eta\gamma^2)}}$	$\left\{0,1,-\frac{(1+4\eta\gamma)\xi\mathrm{i}}{1+4\eta\gamma+4\eta\gamma^2}\right\}$
r	-	$\{0,0,1\}$

in Table 1 and 2, where $\gamma=a_2/a_1$ and $\eta=h/k$. Also, wave modes corresponding to $\{u_1,u_2,\theta_3\}$ including rotational wave (r-wave) is observed.

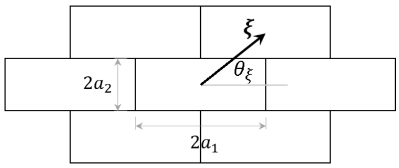

Fig. 2: A single layered 2 dimensional brick arrangement.

(3) Spin frequency

Based on the continnuumnization, although we cannot determine the finite wave velocity of rotational mode, we are able to determine the frequency of the rotational mode as,

$$\omega_{\text{spin}}=\sqrt{\frac{3ka_1^2+12ha_1a_2+12ha_2^2}{2\rho a_1^2a_2+2\rho a_2^3}} \tag{8}$$

The application of the high frequency spin will be express in the application of the damping.

(4) Estimation of wave properties based on an arbitrary order approximation

In the second order formulation given in subsection (1), we used only the terms up to the second order derivatives in Eq. 6. It surely is odd to consider all the infinite number of terms of the Taylor expansion in approximating variables. However strange it sounds, lets do exactly that. This produces a very complex set of equations of motion, which are of no practical use. However, the presence of some series solutions make it is possible to obtain a quite compact characteristic equation when all the infinite terms of Eq. 6 are used.

With a little bit of mathematical manipulations, the following two relations for the Fourier transform of Eq. 6 can be established; note that all the terms in the infinite series are included.

$$\int \left(\boldsymbol{u}^{\gamma+}+\boldsymbol{u}^{\gamma-}\right) e^{\imath(\boldsymbol{\xi}\cdot\boldsymbol{x}-\omega t)}\mathrm{d}\boldsymbol{x}\mathrm{d}t \approx 2\left(1-2\sin^2(\boldsymbol{\xi}\cdot\boldsymbol{r}^\gamma)\right)\hat{\boldsymbol{u}}$$
$$\int (\boldsymbol{u}^{\gamma+}-\boldsymbol{u}^{\gamma-}) e^{\imath(\boldsymbol{\xi}\cdot\boldsymbol{x}-\omega t)}\mathrm{d}\boldsymbol{x}\mathrm{d}t \approx 2\imath\{\sin(2\boldsymbol{\xi}\cdot\boldsymbol{r}^\gamma)\}\hat{\boldsymbol{u}} \quad (9)$$

$\hat{\boldsymbol{u}}$ and $\hat{\boldsymbol{\theta}}$ are the Fourier transform of $\boldsymbol{u}$ and $\boldsymbol{\theta}$ with respect to the kernel $e^{\imath(\boldsymbol{\xi}\cdot\boldsymbol{x}-\omega t)}$. Now, approximating the discrete terms $(\boldsymbol{u}^{\gamma+}\pm\boldsymbol{u}^{\gamma-})$ and $\left(\boldsymbol{\theta}^{\gamma+}\pm\boldsymbol{\theta}^{\gamma-}\right)$ with the infinite series expressions in Eq. 6 and taking the Fourtier transform, we can obtain the following set of equations.

$$0=\det\begin{bmatrix} -\omega^2\boldsymbol{M}+\sum_\gamma 4\sin^2(\boldsymbol{\xi}\cdot\boldsymbol{r}^\gamma)\boldsymbol{K}^{\mu\gamma} & 2\imath\sum_\gamma\sin(2\boldsymbol{\xi}\cdot\boldsymbol{r})\hat{\boldsymbol{K}}^{\mu\gamma} \\ -2\imath\sum_\gamma\sin(2\boldsymbol{\xi}\cdot\boldsymbol{r}^\gamma)\left(\hat{\boldsymbol{K}}^{\mu\gamma}\right)^{\mathrm{T}} & -\omega^2\boldsymbol{I}+4\sum_\gamma\left(\cos^2(\boldsymbol{\xi}\cdot\boldsymbol{r}^\gamma)\overline{\boldsymbol{K}}^{\mu\gamma}+\sin^2(\boldsymbol{\xi}\cdot\boldsymbol{r}^\gamma)\overline{\overline{\boldsymbol{K}}}^{\mu\gamma}\right)\end{bmatrix}$$

$\boldsymbol{M}=m\mathbf{1}\mathbf{1}$ is the mass matrix and $\boldsymbol{I}$ is the moment of inertia tensor of a brick; $\mathbf{1}$ is the identity matrix.

The resulting set of equations are complicated and canoot be solved to obtain simple analitical expressions for wave properties. However, we can numerically solve it to find realtion between frequencies and wave numbers; i.e. ω and $\boldsymbol{\xi}$. As it will be shown in the next section, the wave properties predicted with this characteristic function is valid for wider range of wave numbers, compared to those from the second order approximation obtain in section (2). This infinite series solution could be a good candidate for verification of any rigid-body spring codes.

3. Verification of the predicted wave properties

To verify the wave characteristics predicted with continuumnization and identify the applicable range of these predictions, we compared the predicted properties with the results obtained from a Rigid Body Spring Model (RBSM) simulation. We compare the predictions from the following three continuumnization models introduced in the previous section; original proposal of continuumnization (i.e. approximating $\left(\boldsymbol{\theta}^{\gamma+}+2\boldsymbol{\theta}^{\mu}+\boldsymbol{\theta}^{\gamma-}\right)\approx 4\boldsymbol{\theta}^{\mu}$ and all the rest with second order terms), second order approximation introduced in section (1), and infinite series solutions from section (4). For the sake of brevity, we refer these three as original continuumnization (OC), second order continuumnization (SOC), and infinite series continuumnization (ISC).

3.1 Basic problem settings

. A brick wall of width 20.3m and height 13.0m shown in Fig.3 was used for the simulations. The domain consists of bricks with 60mm width, 30mm high, and 40mm thickness[10]. The density of each block is assumed to be 1850kg/m^3. k and h, are determined as $5.12\times10^{11}\,\mathrm{N/m^3}$ and $2.22\times10^{11}\,\mathrm{N/m^3}$, respectively.

For the sake of simplicity, 2D settings is assumed and the domain is subjected to in-plane wave at center of the domain. We considered 3 cases with different input waves. First and second cases are with transnational waves of vertical and horizontal excitation. The third case is with a rotational wave input. In all the cases, following wave form is used.

$$f(t)=\frac{2}{3\sqrt{3}}A\left(\sin\frac{\omega t}{2}-\frac{1}{2}\sin\omega t\right), \qquad (10)$$

where A is the amplitude of the input, ω is the input circular frequency. The amplitude is set to be 2mm for vertical and horizontal inputs, while amplitude of 0.035radian is used for rotational input. To obtain a narrow waves, so that peaks and valleys of waves are clearly visible, input circular frequency ω is set to be 1.57×10^4radian/s for vertical and horizontal input, and 2.11×10^5radian/s for rotational input.

In order to obtain accurate results, we use a second order velocity Verlet algorithm with $1\mu s$ time step for time integration. As an indirect check to make sure the accuracy of the simulation, the energy and the momentum of the whole system is monitored. Near perfect preservation of energy and momentum is observed, indicating that the simulations results have a high accuracy.

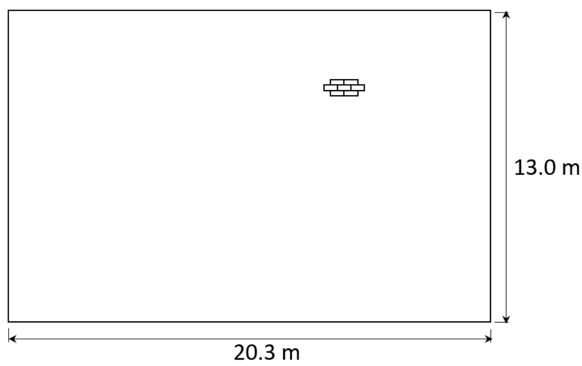

Fig. 3: Domain for the numerical experiments.

3.2 Comparison of translational waves

The color contours of Fig. 4(a) and (b) shows the distribution of translational wave amplitudes at time 2ms. The two white color curves indicates the theoretically predicted location of wave fronts. The outermost indicates the p-wave front, while the innermost indicates the shear wave front. These analytical predictions are obtained with the second order continuumnization model presented in the section (1).

(1) Primary or pressure wave

As is seen, the analytical prediction is in good agreement with numerical results in the regions indicated with letter A. The wave profiles along section P-P, shown in Fig.5 clearly indicates that the analytical predictions are in good agreement with the numerical results. In Fig.4(a), since the input wave is oriented in vertical direction, the p-wave amplitude is strong in up and down directions, while it is weak in other directions. This is why no p-wave front is present in the numerical results except in up and down directions. The nearly straight wave fronts in the region C are the shear shock waves generated by the p-wave front in region A.Being an anisotropic medium, deformation due to p-, s- or rotational waves generates each other. s-waves generated by the p-wave front forms a shockwave, since p-wave speed is higher than s-wave.

(2) Shear-wave

Fig. 4(a) and (b) shows that in the area indicated with letter B the theoretically predicated s-wave fronts are also in good agreement with that of numerical results. Fig.6 provides clear evidences to support this claim. Like in the case of p-wave, amplitudes of the main s-wave is weak in most directions, except in the direction orthogonal to the direction of excitation.Especially, major shear wave in the directions of excitation have extremely small amplitudes. This is why there seems to be a significant mismatch between numerical and analytical wave fronts in regions except A.

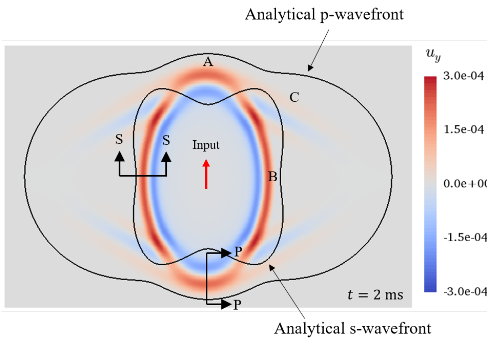

(a) with vertical input

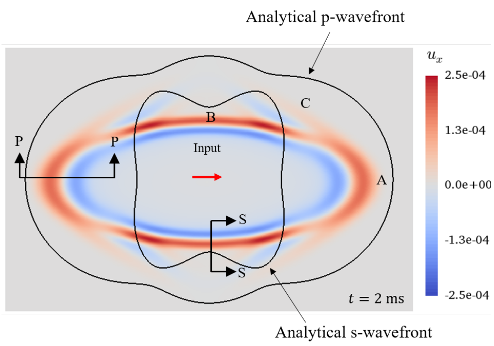

(b) with horizontal input

Fig. 4: Comparison of predicted p- and s-wave fronts with those of numerical results, at 2 ms. The colors indicates the amplitude of translational waves.

(a) Vertical input (b) Horizontal input

Fig. 5: Translational wave profiles, along sections P-P, in the vicinity of p-wave front at 2 ms. The arrows indicates the analytically predicted wave front location.

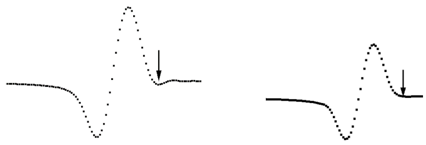

(a) Vertical input (b) Horizontal input

Fig. 6: Translational wave profiles, along sections S-S, in the vicinity of s-wave front at 2ms. The arrows indicates the analytically predicted wave front location.

3.3 Comparison of rotational-waves

Fig. 7 shows the distribution of the amplitudes of rotational waves generated by the rotational wave input, at 2 ms. Unlike the translational wave inputs, the dispersion of the rotational wave occurs. Due to the difficultly of analytically estimate the rotational wave velocity, the double Fast Fourier Transform (FFT) with respect to spatial and time domain was conducted. FFT was conducted for two sets of narrow domains oriented horizontally and vertically; shown with yellow lines in Fig.7.

The results of the double FFTs are shown in Fig.8, 9 and 10. The vertical axis is circular frequency and the horizontal axis is the normalized wave number, where a_1 and a_2 are the half of the length and height of a brick (see Fig.2). Note that the white color regions indicate that the amplitude is beyond the color scale. Red, green, and yellow color curves represent the analytical solutions for p-, s- and r-waves, respectively. It is observed that there is not only r-wave, but also small amplitude p- and s-wave are also present. This gives us a good opportunity to make a further detailed comparison between the predicted p- and s-wave properties with those from the numerical results.

We compared the analytical results obtained from the three continuumnization models with the numerical results. In Fig.8, analytical solutions are obtained from the original continuumnization proposed by Hori et al.[1)] (i.e. OC). As It is seen that the rotational frequency matches the analytical results only in a small neighborhood of $|\xi a_1|=|\xi a_2|=0$. When we move away from this small neighborhood, the analytical predictions start to diverge rapidly.

In Fig.9, analytical solutions are obtained from the second order continuumnization presented in section (1) (SOC). Due to the increase in order of the approximation of the relative rotation, it is seen that the numerical solution is in good agreement in the ranges $|\xi a_1|<0.5$ and $|\xi a_2|<0.5$. In other words, the the 2^{nd} order Taylor based continuumnization is valid for the wavelength is grater than 7 times of the size of bricks. One interesting observation is that the s-wave predictions start to diverge rapidly outside the ranges $|\xi a_1|<0.5$ and $|\xi a_2|<0.5$. On the other hand, such large divergence of s-wave predictions does not occur with the original continuumnization model OC.

The advantage of the continuumnization with the infinite order approximation is clearly seen in Fig.(10). Analytical predictions for s- p- and rotational waves are in near perfect agreement with the numerical results for a whole range of wave numbers considered. We limited our analysis to the range $\xi a \leq 1.5$ since it corresponds to the shortest meaningful wavelength for the considered problem; $\xi a \leq 1.5$ includes wavelengths larger two times the respective dimension of a brick.

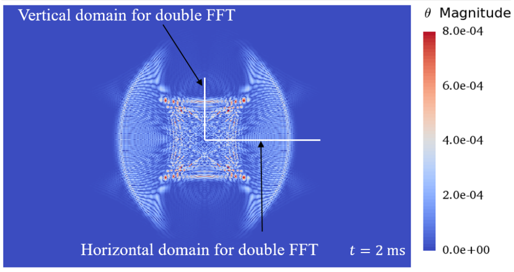

Fig. 7: Magnitude of the rotational waves at 2 ms, generated by rotational wave input. Two white lines indicates the thins domains used for double FFT.

3.4 Continuumnization as a verification tool for RBSM simulators

As demonstrated in the above set of simulations, continuumnization can predict the wave characteristics accurately. These prediction could be an excellent benchmark problems for verification of RBSM codes. While the original continuumnization model proposed in [1] can predict wave properties accurately for very small wave numbers, the second order continuumnization model of section(1) is valid for a reasonably wide range of wave numbers. For most of the applications, the second order model could be sufficient. For the applications involving higher frequencies, the predictions from the infinite order model should be used. The authors think that using the infinite series model could be the best choice in verification of numerical codes, since it will clearly indicate in which range a numerical codes is accurate.

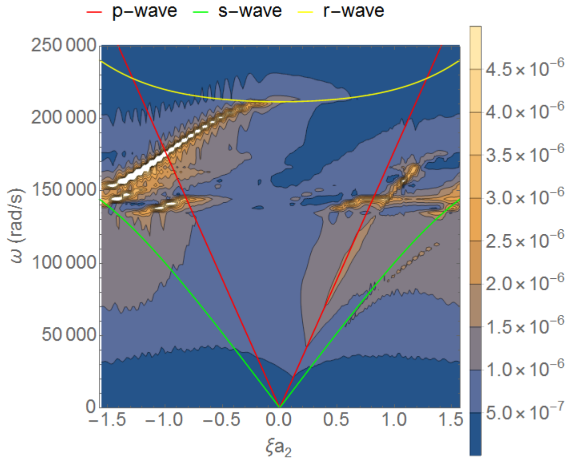

(a) Along the vertical domain

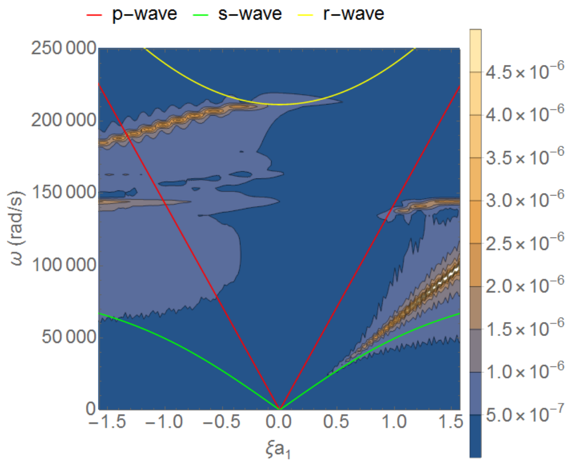

(b) Along the horizontal domain

Fig. 8: Comparison of numerical results and the analytical predictions from original continnumnization model (OC). Contour plots show the numerically obtained amplitude of ω vs. ξa_i realtion. The curves shows the analytical prediction for p-, s- and rotational waves.

4. High speed spin as a source of damping

It is mentioned by Hori et al.[1] that the high frequency spin can be a possible source of damping in granule materials and brick mortar systems. To explain a possible damping mechanism, lets consider the stone block wall considered in this section. According to the stone block properties, Eq. 8 predicts that spin frequency of the blocks is about 12600 rad/s. Such high frequency vibrations must rapidly decay due to interface friction, non-linear properties of mortar, etc. However, the coupling between translational waves and rotational waves continuously transfer some energy from translational modes to generate rotational

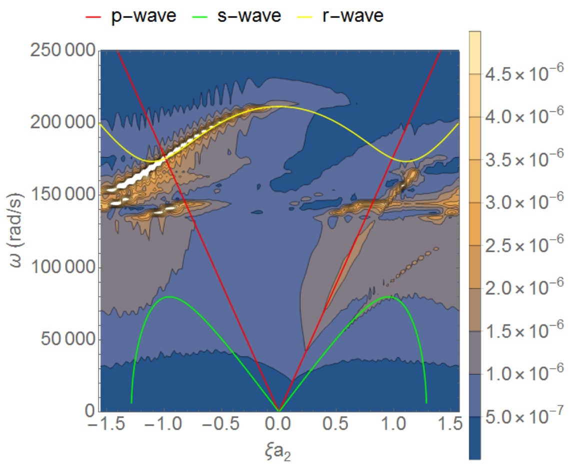

(a) Along the vertical domain

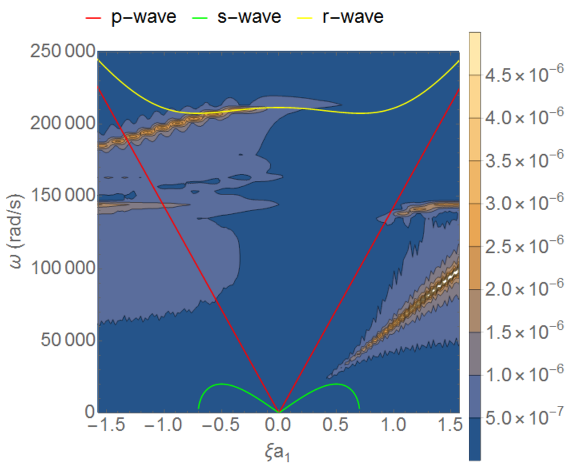

(b) Along the horizontal domain

Fig. 9: Comparison of numerical results and the analytical predictions from the second order continnumnization model (SOC). Contour plots show the numerically obtained amplitude of ω vs. ξa_i realtion. The curves shows the analytical prediction for p-, s- and rotational waves.

waves. Eventually, the system should continuously loose energy producing the effect of damping, since the high spin rotations decay rapidly. While this is one possible mechanism, there could be other mechanism triggered by high speed spins; e.g. nonlinear effects due to spins.

As a preliminary investigation on possible contribution from predicted high speed spins to damping of brick mortar or granule systems, we studied the effect of rapid decay of spin on the response and total energy of a vibrating stone wall. In this study, we mimicked a set of experiments conducted by Elmenshawi et al.[11].

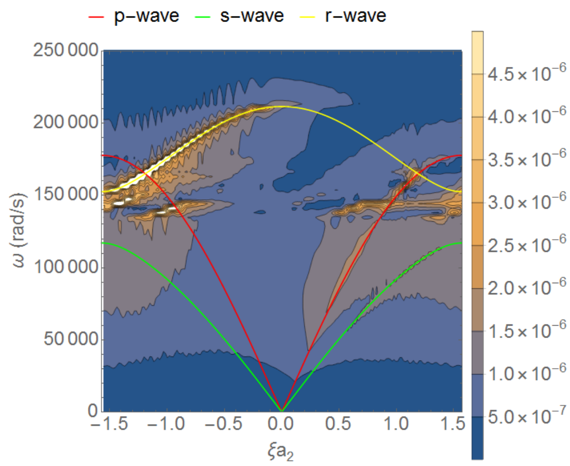

(a) Along the vertical domain

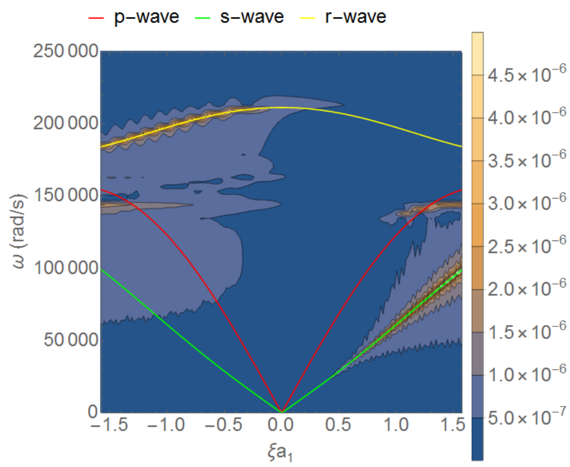

(b) Along the horizontal domain

Fig. 10: Comparison of numerical results and the analytical predictions from continnumnization model with inifinite series (ISC). Contour plots show the numerically obtained amplitude of ω vs. ξa_i realtion. The curves shows the analytical prediction for p-, s- and rotational waves

4.1 Numerical simulation for the rotational damping

To evaluate the influence of the rapid deacy of high frequency spins, a RBSM model of stone brick wall is constructed to mimic the experiments reported by Elmenshawi et al.[11]. The configuration of the wall is shown in Fig. 11. Stiffness k and h are set to be $2.03\times10^{10}\mathrm{N/m^3}$ and $4.69\times10^{8}\mathrm{N/m^3}$, respectively. The density of the bricks is assumed to be $2650\mathrm{kg/m^3}$. The model is initially deformed by subjecting to 9 kN horizontal distributed static force over the top edge (see Fig. 11).. Then the external load over the top edge was suddenly released, and the dynamic response of the wall, at the point A, is observed.

In order to produce rapid decay of high speed spins, a rotational damper is attached to each brick by including the term $-\overline{\boldsymbol{C}}\cdot\dot{\boldsymbol{\theta}}^{\mu}$ into Eq. 4. The resulting discrete governing equations are shown in Eq. (11).

$$
\begin{aligned}
m^{\mu}\ddot{\boldsymbol{u}}^{\mu} &= \sum_{\gamma}\Big\{\boldsymbol{K}^{\mu\gamma}\cdot\left(\boldsymbol{u}^{\gamma+}-2\boldsymbol{u}^{\mu}+\boldsymbol{u}^{\gamma-}\right) \\
&\qquad -\hat{\boldsymbol{K}}^{\mu\gamma}\cdot\left(\boldsymbol{\theta}^{\gamma+}-\boldsymbol{\theta}^{\gamma-}\right)\Big\} \\
\boldsymbol{I}^{\mu}\cdot\ddot{\boldsymbol{\theta}}^{\mu} &= -\overline{\boldsymbol{C}}\cdot\dot{\boldsymbol{\theta}}^{\mu}+\sum_{\gamma}\Big\{\left(\hat{\boldsymbol{K}}^{\mu\gamma}\right)^{\mathrm{T}}\cdot\left(\boldsymbol{u}^{\gamma+}-\boldsymbol{u}^{\gamma-}\right) \\
&\qquad -\overline{\boldsymbol{K}}^{\mu\gamma}\cdot\left(\boldsymbol{\theta}^{\gamma+}+2\boldsymbol{\theta}^{\mu}+\boldsymbol{\theta}^{\gamma-}\right) \\
&\qquad +\overline{\overline{\boldsymbol{K}}}^{\mu\gamma}\cdot\left(\boldsymbol{\theta}^{\gamma+}-2\boldsymbol{\theta}^{\mu}+\boldsymbol{\theta}^{\gamma-}\right)\Big\}
\end{aligned} \tag{11}
$$

In this 2D in-plane problem, we apply in-plane component the damping coefficient, $\overline{C}_{33}$, as

$$\overline{C}_{33}=2\zeta I_{33}\omega_{\mathrm{spin}}, \tag{12}$$

where ζ is the rotational damping ratio, ω_{spin} is the rotational frequency from Eq. 8. I_{33} is the mass moment of the inertia of a brick.

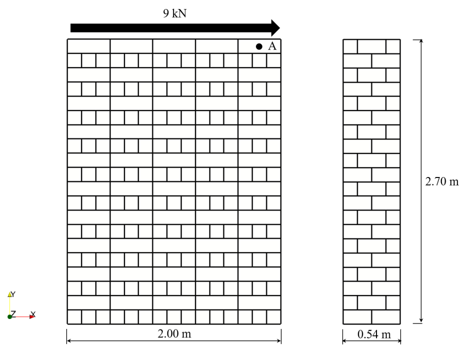

Fig. 11: Brick wall model.

4.2 Energy dissipation in damped free vibration of wall

Fig. 12 shows time history of the total energy of the system with different damping ratios. The near perfect preservation of total energy of the system with $\zeta=0$ is an indirect evidence of the accuracy of the simulations. As is seen, the higher the rate of decay of high speed spin (i.e. higher ζ), the faster the loss of energy of the system. The continuous loss of energy is due to the interplay between the rotational and translational modes via the coupling terms $\hat{\boldsymbol{K}}^{\mu\gamma}\cdot\left(\boldsymbol{\theta}^{\gamma+}-\boldsymbol{\theta}^{\gamma-}\right)$ and $\left(\hat{\boldsymbol{K}}^{\mu\gamma}\right)^{\mathrm{T}}\cdot\left(\boldsymbol{u}^{\gamma+}-\boldsymbol{u}^{\gamma-}\right)$ in Eq. (4) (or $\boldsymbol{q}:\nabla\boldsymbol{\theta}$ and $\boldsymbol{q}^{\mathrm{T}}:\nabla\boldsymbol{u}$ in Eq. (7))

4.3 The decay of the acceleration amplitude

Fig. 13 represents the time history of the horizontal acceleration of the brick at the point A (see Fig. 11), for $\zeta=0.05$. As a result of the rapid decay of high frequency spin and the coupling between rotational and transnational degrees of freedoms, the amplitude of translational acceleration continually decays. These

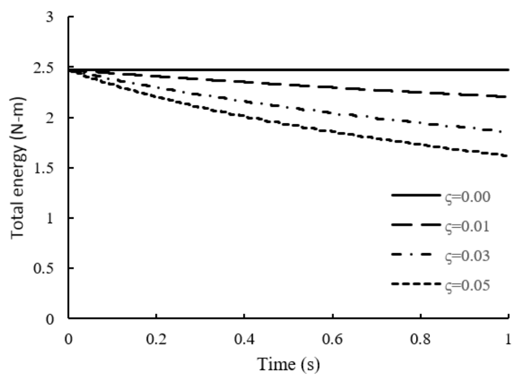

Fig. 12: Time history of the total energy with different ζ.

results are qualitatively somewhat close to the observations by Elmenshawi et al.[11].

The high frequency components at the beginning is due to the instantaneous release of the external force in the numerical model. Such high frequency terms are not observed in the observations by Elmenshawi et al.[11] probably because the external load is not release instantaneously in the real experiment and accelerometers have limited sampling rate. However, after 0.5s, the frequency and the amplitude of the wave profile of the numerical results are comparable to observations by Elmenshawi et al.[11]. Further investigations are necessary to conclude the contribution of predicted high speed spin on system damping.

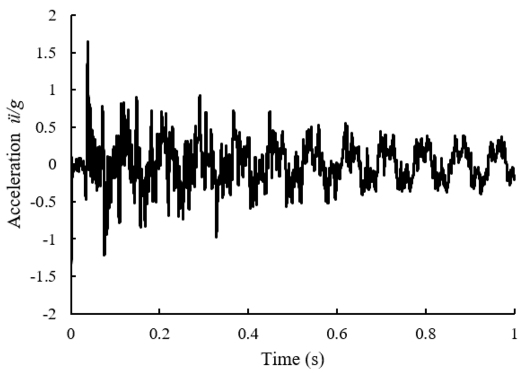

Fig. 13: The horizontal acceleration at point A, with $\zeta=0.05$.

5. Concluding remarks

We developed an equivalent continuum forms for brick structures based on continuumnization and demonstrated that those can be used for verification of Rigid Body Spring Models (RBSM). In this work, we took a slightly different approach form the original proposal by Hori et al.[1] in deriving continuum models. Approximating the discrete vector fields with Taylor series expansion, we obtained two continnumnized models for predicting wave properties; one based on second order approximation, while the infinite series is used for the other. With numerical simulations, it is demonstrated that continuumnization can accurately predict the properties of p-, s- and rotational waves making it good tool for verification of RBSM codes. Comparison of these continnumized modes shows the second order model is valid for a reasonably wide range of wave numbers and sufficient for most applications. For applications involving high frequencies, predictions from the infinite order model can be used.

A preliminary investigation is conducted on possible contribution from predicted high speed spins to damping of brick mortar or granule systems. It is demonstrated that rapid decay of high predicted high speed spin and the interplay between translation and rotation mode can produce significant energy loss and damping of translational responses. While the numerical simulations produced results comparable to observations by Elmenshawi et al.[11)], further investigations are necessary to conclude the contribution of predicted high speed spin on system damping.

REFERENCES

1) Hori, M., Wijerathne, L., Chen, J., and Ichimura, T.: Continuumnization of regularly arranged rigid bodies, *Journal of JSCE*,Vol. 4, pp. 38-45, 2016.
2) Portiolia, F., Casapullaa, C., Gilbertb, M., Cascinia, L.: Limit analysis of 3D masonry block structures with non-associative frictional joints using cone programming, *Computers & Structures*, Vol. 143, pp. 108-121, 2014.
3) Ferris, M.C., Tin-Loi, F.: Limit analysis of frictional block assemblies as a mathematical program with complementarity constraints, *International Journal of Mechanical Sciences*: Vol. 43(1), pp. 209-224, 2001.
4) Casapulla, C. and Portioli, F.: Experimental and analytical investigation on the frictional contact behavior of 3D masonry block assemblages, *Construction and Building Materials* Vol. 78, pp. 126-143, 2015.
5) Furukawa, A., Kiyono, J., and Toki, K.: Numerical simulation of the failure propagation of masonry buildings during an earthquake, *Journal of Natural Disaster Science*, Vol. 33(1), pp. 11-36, 2012.
6) Orduña, A., Lourenco, P.B.:Three-dimensional limit analysis of rigid blocks assemblages. Part I: Torsion failure on frictional interfaces and limit analysis formulation, *International Journal of Solids and Structures*, Vol. 42, pp. 5140-5160, 2005.
7) Portioli, F., Cascini,L., Casapulla, C., and D'Aniello, M.: Limit analysis of masonry walls by rigid block modelling with cracking units and cohesive joints using linear programming, *Engineering Structures,* Vol. 57, pp. 232–247, 2013
8) Lourenco, P.B. and Rots, J. G.: Multisurface interface model for analysis of masonry structures, *Journal of Engineering Mechanics,* Vol. 123(7), pp. 660-668, 1997.
9) Topping, B.H.V. and Wong, F.L.: Finite element modelling of the sonic method of testing masonry structures, *Computers & Structures*,Vol. 41(1), pp. 109-136, 1991.
10) Wang, S.Y., Sloan, S.W., Abbo, A.J., Masia M.J., and Tang, C.A.:Numerical simulation of the failure process of unreinforced masonry walls due to concentrated static and dynamic loading, *International Journal of Solids and Structures*, Vol. 49(2), pp. 377-394, 2012.
11) Elemenshawi, A., Sorour, M,. Mufti, A. Jaeger, L.G., and Shrive, N.: Damping mechanisms and damping ratios in vibrating unreinforced stone masonry, *Engineering Structures*, Vol. 32, pp. 3269-3278, 2010.